ACS Sustainable Chemistry & Engineering

Research Article

pubs.acs.org/journal/ascecg

Trash to Treasure: Transforming Waste Polystyrene Cups into Negative Electrode Materials for Sodium Ion Batteries

Weliton Silva Fonseca, Xinghua Meng, and Da Deng*

Department of Chemical Engineering and Materials Science, Wayne State University, Anthony Wayne Drive, Detroit, Michigan 48202, United States

Supporting Information

ABSTRACT: Modern society generates a huge amount of plastic wastes that are posing potential disasters to our environment and society. For example, waste polystyrene (PS), such as used PS cups and packing materials, is mainly disposed into landfills. It is very challenging to recycle PS economically. PS cannot be carbonized under conventional conditions, because PS is completely decomposed into toxic gases at moderate temperature instead of carbonization. Here, we demonstrated a facile procedure to transform waste PS cups collected from a local coffee shop into disordered carbon in a sealed reactor at moderate temperature but under high pressure. The as-obtained disordered carbon demonstrated interesting electrochemical characteristics for reversible storage of sodium ions. A highly reversible capacity of 116 mAh g^{-1} could be achieved for at least 80 cycles. Our preliminary results demonstrated that the trash of waste PS cups could be facilely transformed into treasure of promising negative electrode materials for sodium ion batteries, offering an alternative and sustainable approach to manage the waste PS issue.

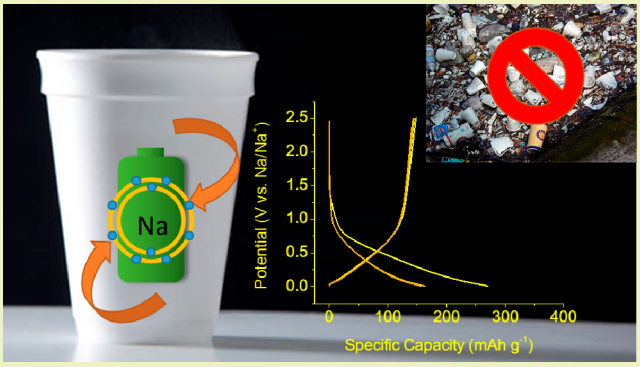

KEYWORDS: *Polystyrene, Carbonization, Amorphous carbon, Anodes, Sodium ion batteries*

INTRODUCTION

The modern society generates a huge amount of waste plastics that, if not properly managed, can pose severe global environmental problems.[1−3] For example, sea animals (sea turtles,[4,5] sea birds,[6,7] fishes[8] and manatees[9]) are being threatened by discarded nonbiodegradable waste plastics.[10,11] In the United States, 41 million tons of waste plastics were generated in 2011 according to the report from Earth Engineering Center.[12] Currently, waste plastics are mainly landfilled (83.4%), or incinerated with a fraction of energy recovered as electricity and fuel (10.1%) and only 6.5% waste plastics are recycled. The current approaches in managing plastic wastes have a few notable issues. The low density waste plastics can quickly take up the limited landfill space. Additionally, the plastics in landfill, without exposure to UV and microbes, may take hundreds of years to be degraded. Waste plastic recycling is not economically viable because of the high cost associated with collecting and sorting processes. The waste plastics have to be washed to remove labels and print, which may generate other wastes, such as wastewater and organic solvents. The incineration process also has issues, including toxic gases and CO_2 released and contributing to air pollution and climate changes. The incineration process is not carbon neutral. Therefore, it will be highly beneficial from both the environmental and energy conservation points of view to develop innovative solutions to transform waste plastics into high value products by carbon recycling, such as electrodes for rechargeable batteries.

The transformation of waste plastics into high value products is attracting much attention recently. A number of carbon materials with different structures have been obtained from waste plastics. For example, carbon nanotubes have been derived from thermal decomposition of low density polyethylene (LDPE) or polypropylene (PP) after mixing with catalysts (cobalt acetate or iron nanoparticles, respectively) at 700 °C.[13,14] Carbon spheres have been prepared by carbonizing LDPE, high density polyethylene (HDPE), polyethylene terephthalate (PET) or polystyrene (PS) under autogenic pressure at 700 °C.[15] Polyethylene (PE) and Polyvinyl chloride (PVC) have also been used to form carbon spheres under high pressure (30 MPa) at 650 °C.[16] Besides, carbon nanofibers have been derived from PE with the mixed catalysis of CuBr and NiO at 700 °C.[17] Among various carbon transformation methods, carbonization under high pressure is an emerging approach to convert waste plastics into valuable carbon materials.[13,18,19] Inagaki et al. first demonstrated that it was feasible to obtain carbon spheres by pressure carbonization treatment of PE, PP and PVC at a moderate temperature of 650 °C under a pressure of 30 MPa.[16,20,21] Pol et al. explored the

Received: May 7, 2015
Revised: July 14, 2015
Published: July 21, 2015

DOI: 10.1021/acssuschemeng.5b00403
ACS Sustainable Chem. Eng. 2015, 3, 2153−2159

direct carbonization of waste plastics by high pressure carbonization.[22,23] Although the carbonization of various waste plastics has been explored, the carbonization of waste PS (popularly used for disposable cutlery, boxes and cups) and the applications of the PS derived carbon is relatively rarely studied.[15,24]

PS cannot be recycled economically and are nonbiodegradable. About 3 million tons of expanded PS are produced annually in the world and 70% of the expanded PS is used as single-use food packing and is disposed into our environment.[25] Disposed PS is typically landfilled, which takes about 25%−30% of the space of landfills. PS should not be incinerated, because the decomposed gases of polycyclic aromatic hydrocarbons (PAHs) are extremely toxic.[26] Unlike other polymers, such as PE and PET with recycle rates up to 90%, the recycle rate of PS is insignificant. Besides, recycle of PS is a low-profit business and cannot attract continuous commercial investment. For example, Sony tried to recycle PS, but failed due to the low value of recycled PS and high cost of PS collection and storage.[27] New York City, Seattle, Portland, San Francisco and Washington DC have already banned the use of PS food and beverage containers. Therefore, instead of recycling, transformation of PS into high value carbon materials could be a more attractive and sustainable option. However, the conventional carbonization of PS is impossible. This is because PS is completely decomposed into small molecules (e.g., PAHs) at the moderate temperature of 450 °C,[28] far below the minimum temperature required for carbonization of polymers at above 600 °C.[29] Instead of direct carbonization of PS, PS-based macroreticular resins have been carbonized and the carbon derived could be used in supercapacitors,[30] and to remove pollutants.[31] Jian et al. carbonized PS with mixed catalysts (OMMT/Cobalt) to obtain porous carbon spheres, which could be used as catalyst supports, adsorbents, storage materials and new templates for carbon materials.[32] Li et al. prepared hollow carbon spheres by carbonizing cross-linked PS with the aid of $AlCl_3$ and CCl_4.[33] Wu et al. coated PS with sewage sludge during pyrolysis process to get hollow carbon spheres to adsorb organic pollutants in water.[34] The carbonization PS under high pressure without any catalysts or matrices was reported before.[15] However, the application of directly carbonizing PS for sodium ion batteries (SIBs) has not been reported.

Herein, we reported the derivation of disordered carbon from waste PS cups by carbonization under high pressure for SIBs. The effects of carbonization temperatures on the carbon derived and their electrochemical performances, in relevance to carbon structure and degree of graphitization, were studied. Our preliminary results demonstrated that the waste PS-derived carbon materials, obtained by simply heating to 700 °C, could deliver highly reversible capacity of ~116 mAh g^{-1} for at least 80 cycles with nearly 100% Coulombic efficiency. Therefore, our results suggest that waste PS could be a rich source of disordered carbon used in future SIBs, providing a sustainable option to solve the issue of waste PS.

EXPERIMENTAL SECTION

Materials Preparation. Typically, 400 mg of PS, cut from a PS cup from a local coffee shop on campus, was inserted in a 4 mL reactor (constructed by stainless steel Swagelok fittings) at room temperature in argon inside a glovebox. The reactor was sealed and heated in air. The ramp rate was set at 20 °C min^{-1}, and then held at 500, 600 or 700 °C for 3 h before cooled down naturally. The black solid collected after reaction was washed by acetone and water and dried in an oven overnight at 50 °C. The amount of solid sample obtained after reaction at 500 °C was insignificant and was not extensively analyzed. The solid samples obtained from 600 and 700 °C reactions were denoted as PS600 and PS700, respectively, and were extensively characterized.

Materials Characterization. The degree of carbonization was characterized by X-ray powder diffraction (XRD, Rigaku, with Cu Kα radiation) and Raman by the E-Z Raman spectroscopy system at room temperature. The morphologies of the carbon derived from PS were characterized by a field-emission scanning electron microscopy (FESEM, JEOL-7600). A thermogravimetric analysis (TA Instrument, SDT Q600) was carried out from room temperature to 800 °C at ramp rate of 20 °C min^{-1} in air.

Electrochemical Measurement. Typically, the black color carbon samples derived from PS as active materials were mixed with Super-P carbon black, PVDF binder at the mass ratio of 8:1:1 in a NMP solvent. The homogeneous slurry was coated on Cu foils as current collectors and dried in a vacuum oven at 100 °C overnight. The CR2032 coin cells were assembled in Argon filled glovebox with metallic sodium foils as negative electrodes and Celgard 3501 separators filled with an electrolyte (1 M $NaClO_4$ in a mixture solvent of ethylene carbonate and diethyl carbonate with the volume ratio of 1:1). The coin cells were tested galvanostatically at room temperature. The voltage window was set at 0.01−2.5 V at the current of 20 mA g^{-1}

RESULTS AND DISCUSSION

We observed that the temperature could significantly affect the carbonization of PS. As illustrated in Figure 1, we observed that

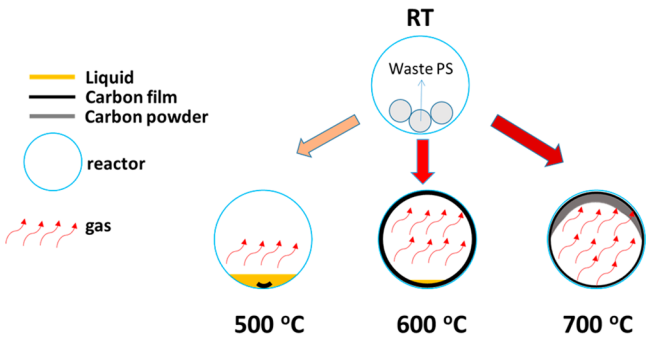

Figure 1. Schematic to show the location of carbon deposition observed inside the sealed reactor after carbonization at different temperatures (500, 600 and 700 °C).

mainly yellow to brown and oily liquid, pitch-smelled gases and insignificant amount of solid were inside the reactor upon opening after treatment at 500 °C (Figure S1a in the Supporting Information). In contrast, a thick layer of carbon film was deposited inside the reactor after treatment at 600 °C. We observed that the carbon film peeled off from the reactor had a shiny and smooth texture on the side in contact with the stainless steel reactor, and the other side of the carbon film had a dark and highly rough texture. After heat treatment at 700 °C, we observed carbon film was deposited on the inner wall of the reactor, similar to that obtained at 600 °C, and also a thick layer of carbon powder on the film. The amount of oily liquid observed in the last two cases was minimum (Figures S2 and S3 in the Supporting Information), suggesting that high carbonization efficiency could only be achieved above 500 °C.

We used XRD to analyze the carbon materials derived from PS at 600 and 700 °C (Figure 2a). Two typical broad peaks at around 25° (24.9° for PS600 and 25.1° for PS700) and 43° (43.0° for PS600 and 43.2° for PS700) could be associated with diffraction from graphite planes (002) and (100).[35,36] The

DOI: 10.1021/acssuschemeng.5b00403
ACS Sustainable Chem. Eng. 2015, 3, 2153−2159

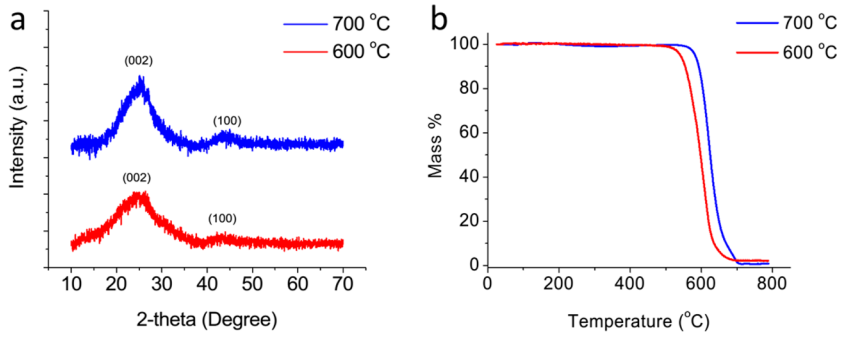

Figure 2. (a) XRD patterns and (b) TGA curves of as-prepared carbon materials after carbonizing PS at 600 and 700 °C for 3 h.

broad diffraction peaks suggested their low degrees of graphitization. The carbon obtained at 700 °C showed relatively stronger peak intensity and slightly reduced interlayer spacing as compared to that obtained at 600 °C, suggesting slight improved degree of graphitization. High temperature can improve the degree of carbonization because of the progressive removal of hydrogen atoms and improved ordering in stacking structure of extended aromatic layers.[37−39] However, the carbonization temperature of 700 °C is still relatively low, leading to low degree of carbonization. In other words, it is still considered as mainly disordered carbon with defects, voids, and edges, in contrast to that of ordered graphite. The calculated graphitic interlayer spacing (d_{002}) based on Bragg's law is 0.357 and 0.354 nm for PS600 and PS700, respectively. They are both larger than that of graphite (0.334 nm). The disordered carbon structures, with large interlayer spacing, low graphitization, disordered graphene arrangement, and presence of voids, are highly beneficial for sodium ion storage. In fact, graphite cannot reversibly store any significant amount of sodium ions (less than 5 mAh g^{-1}), in contrast to that of lithium ion storage (372 mAh g^{-1}).

The thermal stability of the obtained carbon was also evaluated by TGA in air (Figure 2b). The carbon derived at 600 °C started to decompose at ∼478 °C and stabilized at ∼681 °C, with total mass loss of 98.4%. With the increase of carbonization temperature, carbon obtained at 700 °C demonstrated better thermal stability, which started to decompose at ∼535 °C and stabilized at ∼706 °C, with total mass loss of 99.2%. The higher oxidization temperature of PS700 than that of PS600 suggests a better thermal stability of the former due to higher degree of graphitization than the later. The pressure generated and the amount of hydrogen released from hydrocarbon inside the reactors could be different at different temperature, which can affect the degree of graphitization and thermal stability.[15,40,41] The remained mass at 800 °C after TGA scan is ∼1.56% for PS600, which is slightly higher than that of PS700 at ∼0.78%. The difference in remained masses for PS600 and PS700 after oxidization could be plausibly rationalized. It is known that various small amount of additives are typically used in the process of production of PS productions, including antioxidants, UV stabilizers, fillers, pigments, processing lubricants, antistats and flame retardants. Therefore, the remained masses could be from the additives. Given that PS700 has higher carbonization efficiency than that of PS600, or more carbon derived from PS, the percentage of the remained masses of additives after oxidization of carbon should be lower for PS700.

Raman spectra were also used to characterize the degree of graphitization of the PS derived carbon (Figure 3). For

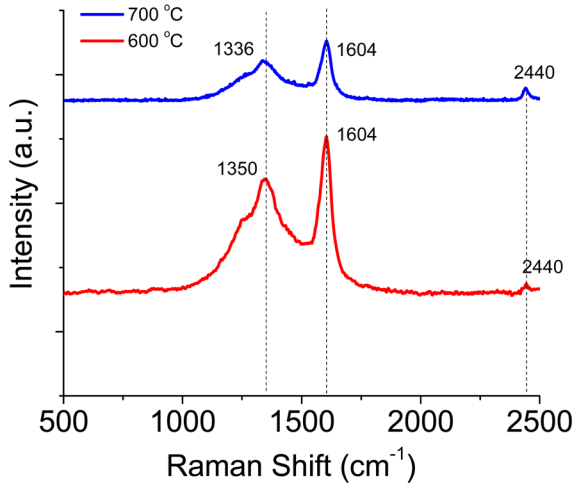

Figure 3. Raman spectra of as-prepared PS600 and PS700 after carbonizing PS at 600 and 700 °C for 3 h.

disordered carbon materials, there are two typical peaks: The G-band is related to graphitized carbon associated with sketching motion of pairs of sp^2-bonded carbons in 2D hexagonal lattice; The D-band is associated with diamond-like disordered carbon. For graphite, there is only one sharp G-band at around 1580 cm^{-1}.[42] The G-band shifted to higher frequency at 1604 cm^{-1} for the PS derived carbon as compared to that of graphite which indicates formation of nanocrystalline graphite.[43,44] There is a shift in D band from 1350 cm^{-1} for PS600 to 1336 cm^{-1} for PS700. The shift to lower frequency could be attributed to phonon-confinement effects associated with curvature and uneven distribution of graphite-atom planes.[45] A shoulder peak at ∼1250 cm^{-1} was observed which is related to defects or graphite domains less than 20 nm.[46] A small peak appears at 2440 cm^{-1} was observed that could be attributed to the second-order Raman spectrum of graphite.[47] The relative intensity I_D/I_G reflects the degree of disorder in the carbon materials. The I_D/I_G ratios of PS600 and PS700 were 0.728 and 0.730, respectively. On the basis of the I_D/I_G ratios, we calculated that the average width (La) of graphitic crystalline of PS600 and PS700 were about 6.02 and 6.04 nm.[48,49] Therefore, based on XRD and Raman analysis, we conclude that disordered carbon was successfully derived from waste PS cups.

The morphology of the carbon products derived from PS after carbonization at 600 and 700 °C were revealed by both optical images and FESEM images (Figure 4). For PS600, carbon film was peeled off from the wall of the reactor in the form of broken flakes (Figure 4a and Figure S2 in the Supporting Information). The surface of carbon film in contact

DOI: 10.1021/acssuschemeng.5b00403
ACS Sustainable Chem. Eng. 2015, 3, 2153−2159

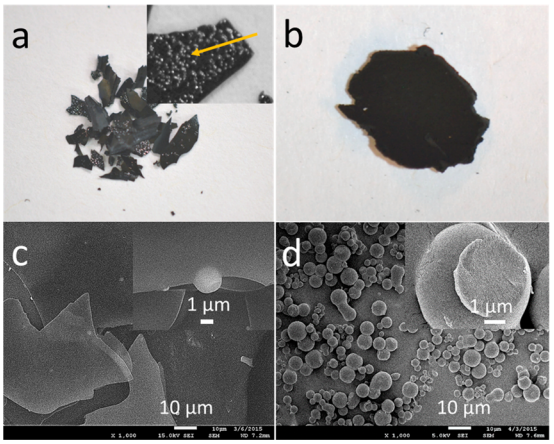

Figure 4. Optical images (a, b) and FESEM images (c, d) of solid carbonized products after carbonization at different temperature: (a, c) carbon film peeled off from the wall of reactor after carbonization of PS at 600 °C, (b, d) carbon film with aggregated carbon powder peeled off from the wall of reactor after carbonization of PS at 700 °C. Inset of panel a is the optical image showing the rough surface of the carbon film not in contact with the wall of the reactor. The insets in panels c and d are the high magnification FESEM images to show details of micromorphologies of the carbon obtained.

with the wall of the reactor was smooth duplicating the smooth surface of the reactor, whereas the other side of the carbon film was highly rough (inset of Figure 4a). The smooth surface was attributed to the carbon-stainless steel interface. The rough surface could be attributed to the solidified liquid–gas interphase that eventually carbonized under high pressure and high temperature conditions. Occasionally, carbon spheres with size about 2.2 μm were also observed (inset of Figure 4c). For PS700, the main product is carbon spheres (Figure 4b,d). The byproduct, carbon film, was observed as well (Figure S3d in the Supporting Information), on which a thick layer of carbon powder deposited. The optical images of carbon spheres, attached on carbon film forming a piece of flake are shown in Figure 4b. For Figure 4b, the rough surface without any reflection indicates that the porous carbon layer is composed of carbon spheres which absorb light. The size of carbon spheres ranges from 1 to 8 μm, as shown in Figure 4d. The carbon spheres are aggregated. Inagaki et al. have reported that there was no carbon derived from carbonization of PS observed up to 650 °C under 30 MPa in a sealed and thin-walled gold capsule inside an heated pressure bomb or under isostatic pressure.[50] But we could obtain collected carbon phase at 600 °C here based on our closed system. To understand the difference, we explored a series of samples obtained at different temperature from 500, 600 to 700 °C. After carbonization at 500 °C, there was no obvious solid product collected. Minimum amount of yellow liquid was also observed in the case of PS600 and PS700. The formation of liquid phase suggests that the long polymer chains have been broken or decomposed. It is known that, at 450 °C under atmosphere pressure, PS could be decomposed and release hydrocarbons and hydrogen.[24] Inside a closed reactor, released hydrocarbons gas could be condensed forming liquid upon cooling.

We try to rationalize the possible carbonization mechanisms involved. During the early stage of carbonization of PS, PS could be thermally decomposed into low molecular weight liquids and gases under pressure. The original PS molecular weights might have no influence on carbon formation since the degradation of PS into liquid and gas phases occur before the carbonization process.[24] The internal texture of carbon spheres (inset of Figure 4d) is similar to that observed by Pol et al. in the carbonization of PET and PE at 700 °C under autogenous pressure.[22,41] Above critical temperature, hydrogen and hydrocarbon gases might be released from the decomposition of PS. The ratio of hydrogen and hydrocarbon gases could vary before carbonization at different temperature. The phase mixture (gas, liquid and solid) would be different which might determine the

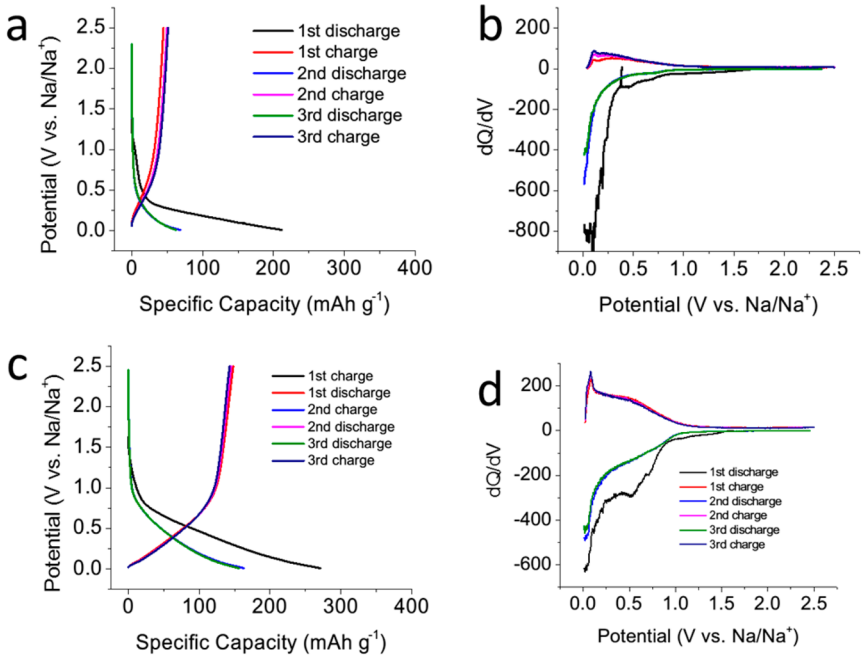

Figure 5. First three cycles of charge–discharge profiles (a, c) and the corresponding dQ/dV plots (b, d) of the as-prepared disordered carbon derived from waste PS for sodium ion storage: (a, b) PS600 and (c, d) PS700. The testing current was 20 mA g^{-1}.

DOI: 10.1021/acssuschemeng.5b00403
ACS Sustainable Chem. Eng. 2015, 3, 2153–2159

products obtained in our PS carbonization as illustrated in Figure 1. The pressure generated could be different at different heating temperature as well. It is challenging to directly measure the pressure precisely inside the rector. In a simplified estimation, we assumed the polystyrene was decomposed to styrene molecules at the set temperature, and other gas products and intermediates were not taken into our calculation. The pressure was roughly estimated to be 7.04 MPa for using 400 mg PS at 700 °C. Similarly, the pressure was estimated to be 5.93 MPa for the case of PS600. We also demonstrated that it is feasible to deposit carbon directly on to Ni foam and Cu foil by carbonization of PS (Figures S4 and S5 in the Supporting Information), which can be directly used as electrodes for supercapacitors and batteries.

The first three cycles of charge−discharge profiles and the corresponding dQ/dV plots of the carbonized PS for SIBs are shown in Figure 5. In the first discharge process, PS600 and PS700 delivered 211.5 and 271.3 mAh g^{-1}, respectively (Figure 5a,c). For PS600 (Figure 5a), a potential drop from open cell voltage to about 0.68 V suggests the Faradic capacitance on the surface or edge sites of carbon layers of disordered carbon is minimum.[51] The potential drop region from 0.68 to 0.38 V suggests the formation of solid-electrode interphase (SEI).[35,52,53] And then a sloping potential drop, ranging from 0.38 to 0.01 V, indicates the insertion of Na ions into graphene layers[54−56] and nanopores.[18,57] In the following charge process, a capacity of ∼50.1 mAh g^{-1} was released. The initial Coulombic efficiency was only 21.1%. There are at least possible three reasons: (1) SEI layer formed on the surface;[58] (2) some Na ions with restricted mobility were trapped inside the voids and pores of the carbon;[59] (3) irreversible side reactions related to trace amount of hydrocarbons and residual hydrogen.[39,56] In comparison, PS700 performed significantly better for storing Na ions. The first discharge profile involves three potential regions: (1) a potential drop before open cell voltage to about 0.85 V, with a capacity contribution of 19.1 mAh g^{-1}; (2) a slope between ∼0.85 and 0.21 V, with a capacity contribution of 200.0 mAh g^{-1}; (3) an indistinct plateau between 0.21 and 0.01 V, with a capacity contribution of 51.9 mAh g^{-1}. The three potential regions could be similarly assigned to those sodium insertion mechanisms discussed for PS600 above, but at slight different positions and significantly different capacity contributions for each region. The first charge capacity was 148.1 mAh g^{-1}. The initial columbic efficiency is 52.8%, which is much better than that in PS600. The improve performance of PS700 as compared to PS600 could be attributed to the formation of nanopores,[55] the removal of residual hydrogen, and the increasing number of graphene layers for reversible insertion of sodium ions.[39] BET analysis showed that the PS700 has a surface area of 88 m^2/g and the size of micropores is about 4 nm (Figure S6 in the Supporting Information). The large surface area is rarely observed in other carbon materials derived based on similar reactor systems which have a surface area about 2−4 m^2/g only.[18,22,40,60] The overlapping curves in the following charge−discharge profiles suggest the highly reversible insertion and extraction of Na ions after the first charge−discharge process. To interpret better the electrochemical results obtained, the dQ/dV plots were plotted (Figure 5b,d). The pair of sharp peaks below 0.2 V could be attributed to the reversible insertion of sodium ions into nanopores. The broad peaks around 0.5 V could be attributed to the reversible insertion of sodium ions between graphene layers.

The cycling performances of PS600 and PS700 are shown in Figure 6. The reversible specific capacity of PS700 is much

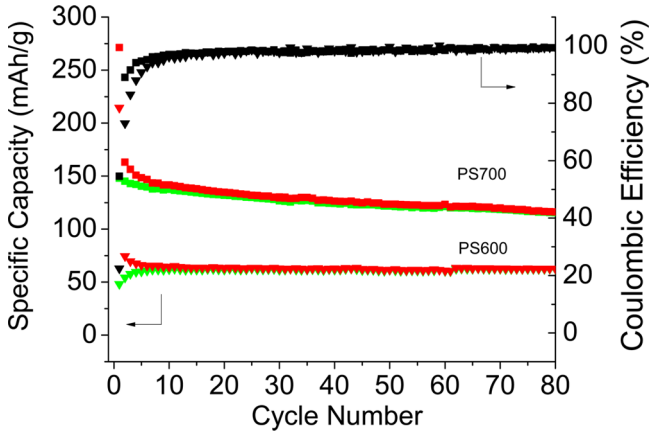

Figure 6. Cycling performances of the as-prepared PS600 and PS700 after carbonizing PS at 600 and 700 °C.

higher than that of PS600. After 80 cycles, PS700 still possesses ∼116.1 mAh g^{-1}. In contrast, PS600 just has ∼62.8 mAh g^{-1}. This observation could be attributed to different carbon structures discussed previously. Their Coulombic efficiencies are rapidly increase from initial low value (21.1% for PS600 and 52.8% for PS700), and stabilized at ∼99% after first 10 cycles. Notably, PS600 has relatively low reversible capacity, but the Coulombic efficiency is slightly better than that of PS700, at 99.5% and 99.2% after 80 cycles, respectively. There could be an optimized carbonized temperature, where the carbon could be fully activated for sodium ion storage. For example, treatment at higher temperature after carbonization could improve the carbon structure for better electrochemical performances.[35,61] Our ongoing effort is focusing on those directions to better understand the structure-performance relationships and to further optimize the carbon derived from PS for sodium ion batteries.

SUMMARY

In conclusion, we demonstrated a simple method to carbonize waste PS cups collected from a coffee shop at 700 °C under high pressure for application as negative electrode materials for SIBs. The effect of temperature and the possible mechanism of forming these carbon materials were discussed. It delivered a stable capacity ∼116.1 mAh g^{-1} at a testing current of 20 mA g^{-1} for at least 80 cycles. We demonstrate an alternative option to transform the waste PS into functional materials which can be used for the production of highly efficient electrodes for SIBs, offering a sustainable approach to handle waste plastics.

ASSOCIATED CONTENT

Supporting Information

Optical image of PS500; optical and FESEM images for PS600 and PS700; optical and FESEM images of carbon coating on Ni and Cu substrates; Raman spectrum of carbon deposited on Cu substrate; BET analysis of PS700. The Supporting Information is available free of charge on the ACS Publications website at DOI: 10.1021/acssuschemeng.5b00403.

DOI: 10.1021/acssuschemeng.5b00403
ACS Sustainable Chem. Eng. 2015, 3, 2153−2159

AUTHOR INFORMATION

Corresponding Author

*Da Deng. E-mail: da.deng@wayne.edu.

Author Contributions

D.D. generated the idea to recycle waste plastics for SIBs; W.S.F., X.M. carried out the experiments; X.M. characterized the samples; D.D. and X.M. analyzed the results and wrote the paper. W.S.F. and X.M. contributed equally.

Notes

The authors declare no competing financial interest.

ACKNOWLEDGMENTS

The authors thank Dr. Stephanie Brock and Dr. Mark Cheng for access to BET and Raman instruments in their laboratories, respectively. The Lumigen Instrument Center, Wayne State University, is appreciated.

REFERENCES

(1) Brems, A.; Baeyens, J.; Dewil, R. Recycling and Recovery of Post-Consumer Plastic Solid Waste in a European Context. *Thermal Science* **2012**, *16*, 669−685.

(2) Hopewell, J.; Dvorak, R.; Kosior, E. Plastics Recycling: Challenges and Opportunities. *Philos. Trans. R. Soc., B* **2009**, *364*, 2115−2126.

(3) Ignatyev, I. A.; Thielemans, W.; Vander Beke, B. Recycling of Polymers: A Review. *ChemSusChem* **2014**, *7*, 1579−1593.

(4) Bugoni, L.; Krause, L.; Petry, M. V. Marine Debris and Human Impacts on Sea Turtles in Southern Brazil. *Mar. Pollut. Bull.* **2001**, *42*, 1330−1334.

(5) da Silva Mendes, S.; de Carvalho, R. H.; de Faria, A. F.; de Sousa, B. M. Marine Debris Ingestion by Chelonia Mydas (Testudines: Cheloniidae) on the Brazilian Coast. *Mar. Pollut. Bull.* **2015**, *92*, 8−10.

(6) Ryan, P. G. Effects of Ingested Plastic on Seabird Feeding - Evidence from Chickens. *Mar. Pollut. Bull.* **1988**, *19*, 125−128.

(7) Vanfraneker, J. A. Plastic Ingestion in the North-Atlantic Fulmar. *Mar. Pollut. Bull.* **1985**, *16*, 367−369.

(8) Carpenter, Ej; Anderson, S. J.; Miklas, H. P.; Peck, B. B.; Harvey, G. R. Polystyrene Spherules in Coastal Waters. *Science* **1972**, *178*, 749−750.

(9) Beck, C. A.; Barros, N. B. The Impact of Debris on the Florida Manatee. *Mar. Pollut. Bull.* **1991**, *22*, 508−510.

(10) Rochman, C. M.; Browne, M. A.; Halpern, B. S.; Hentschel, B. T.; Hoh, E.; Karapanagioti, H. K.; Rios-Mendoza, L. M.; Takada, H.; Teh, S.; Thompson, R. C. Classify Plastic Waste as Hazardous. *Nature* **2013**, *494*, 169−171.

(11) Derraik, J. G. B. The Pollution of the Marine Environment by Plastic Debris: A Review. *Mar. Pollut. Bull.* **2002**, *44*, 842−852.

(12) Themelis, N. J.; Mussche, C. *2014 Energy and Economic Value of Municipal Solid Waste (MSW), Including Non-Recycled Plastics (NRP), Currently Landfilled in the Fifty States*; Earth Engineering Center: New York, 2014.

(13) Pol, V. G.; Thackeray, M. M. Spherical Carbon Particles and Carbon Nanotubes Prepared by Autogenic Reactions: Evaluation as Anodes in Lithium Electrochemical Cells. *Energy Environ. Sci.* **2011**, *4*, 1904−1912.

(14) Chung, Y. H.; Jou, S. Carbon Nanotubes from Catalytic Pyrolysis of Polypropylene. *Mater. Chem. Phys.* **2005**, *92*, 256−259.

(15) Pol, V. G. Upcycling: Converting Waste Plastics into Paramagnetic, Conducting, Solid, Pure Carbon Microspheres. *Environ. Sci. Technol.* **2010**, *44*, 4753−4759.

(16) Inagaki, M.; Kuroda, K.; Sakai, M. Pressure Carbonization of Polyethylene-Polyvinylchloride Mixtures. *Carbon* **1983**, *21*, 231−235.

(17) Gong, J.; Liu, J.; Jiang, Z. W.; Feng, J. D.; Chen, X. C.; Wang, L.; Mijowska, E.; Wen, X.; Tang, T. Striking Influence of Chain Structure of Polyethylene on the Formation of Cup-Stacked Carbon Nanotubes/Carbon Nanofibers under the Combined Catalysis of Cubr and Nio. *Appl. Catal., B* **2014**, *147*, 592−601.

(18) Pol, V. G.; Lee, E.; Zhou, D. H.; Dogan, F.; Calderon-Moreno, J. M.; Johnson, C. S. Spherical Carbon as a New High-Rate Anode for Sodium-Ion Batteries. *Electrochim. Acta* **2014**, *127*, 61−67.

(19) Bazargan, A.; Yan, Y.; Hui, C. W.; McKay, G. A Review: Synthesis of Carbon-Based Nano and Micro Materials by High Temperature and High Pressure. *Ind. Eng. Chem. Res.* **2013**, *52*, 12689−12702.

(20) Washiyama, M.; Sakai, M.; Inagaki, M. Formation of Carbon Spherules by Pressure Carbonization - Relation to Molecular-Structure of Precursor. *Carbon* **1988**, *26*, 303−307.

(21) Inagaki, M.; Kuroda, K.; Inoue, N.; Sakai, M. Conditions for Carbon Spherule Formation under Pressure. *Carbon* **1984**, *22*, 617−619.

(22) Pol, S. V.; Pol, V. G.; Sherman, D.; Gedanken, A. A Solvent Free Process for the Generation of Strong, Conducting Carbon Spheres by the Thermal Degradation of Waste Polyethylene Terephthalate. *Green Chem.* **2009**, *11*, 448−451.

(23) Pol, V. G.; Pol, S. V.; Gofer, Y.; Calderon-Moreno, J.; Gedanken, A. Thermal Decomposition of Tetraethylorthosilicate (Teos) Produces Silicon Coated Carbon Spheres. *J. Mater. Chem.* **2004**, *14*, 966−969.

(24) Ogenko, V. M.; Dubrovina, L. V.; Goldun, O. V.; Volkov, S. V. Porous Inorganic Materials Modified with Pyrolytic Carbon Producted from Polystyrene. *Russ. J. Appl. Chem.* **2007**, *80*, 879−882.

(25) Hearon, K.; Nash, L. D.; Rodriguez, J. N.; Lonnecker, A. T.; Raymond, J. E.; Wilson, T. S.; Wooley, K. L.; Maitland, D. J. A High-Performance Recycling Solution for Polystyrene Achieved by the Synthesis of Renewable Poly(Thioether) Networks Derived from D-Limonene. *Adv. Mater.* **2014**, *26*, 1552−1558.

(26) You, J. H.; Chiang, P. C.; Chang, K. T.; Chang, S. C. Polycyclic Aromatic-Hydrocarbons (Pahs) and Mutagenicity of Soot Particulates in Air Emissions from 2-Stage Incineration of Polystyrene. *J. Hazard. Mater.* **1994**, *36*, 1−17.

(27) Noguch, T.; Miyashita, M.; Watanabe, H. Mechanical Properties of Polystyrene Recycled Using D-Limonene. *Nippon Kagaku Kaishi* **1999**, 615−619.

(28) Jang, B. N.; Wilkie, C. A. The Thermal Degradation of Polystyrene Nanocomposite. *Polymer* **2005**, *46*, 2933−2942.

(29) Inagaki, M.; Kang, F.; Toyoda, M.; Konno, H. *Advanced Materials Science and Engineering of Carbon*; Butterworth-Heinemann: Amsterdam, 2014.

(30) Sun, G. H.; Wang, J.; Li, K. X.; Li, Y. Q.; Xie, L. J. Polystyrene-Based Carbon Spheres as Electrode for Electrochemical Capacitors. *Electrochim. Acta* **2012**, *59*, 424−428.

(31) Wang, Q.; Liang, X. Y.; Qiao, W. M.; Liu, C. J.; Liu, X. J.; Zhan, L. A.; Ling, L. C. Preparation of Polystyrene-Based Activated Carbon Spheres with High Surface Area and Their Adsorption to Dibenzothiophene. *Fuel Process. Technol.* **2009**, *90*, 381−387.

(32) Gong, J.; Liu, J.; Chen, X. C.; Wen, X.; Jiang, Z. W.; Mijowska, E.; Wang, Y. H.; Tang, T. Synthesis, Characterization and Growth Mechanism of Mesoporous Hollow Carbon Nanospheres by Catalytic Carbonization of Polystyrene. *Microporous Mesoporous Mater.* **2013**, *176*, 31−40.

(33) Li, L. C.; Song, H. H.; Chen, X. H. Hollow Carbon Microspheres Prepared from Polystyrene Microbeads. *Carbon* **2006**, *44*, 596−599.

(34) Wu, Z. J.; Kong, L. J.; Hu, H.; Tian, S. H.; Xiong, Y. Adsorption Performance of Hollow Spherical Sludge Carbon Prepared from Sewage Sludge and Polystyrene Foam Wastes. *ACS Sustainable Chem. Eng.* **2015**, *3*, 552−558.

(35) Lotfabad, E. M.; Ding, J.; Cui, K.; Kohandehghan, A.; Kalisvaart, W. P.; Hazelton, M.; Mitlin, D. High-Density Sodium and Lithium Ion Battery Anodes from Banana Peels. *ACS Nano* **2014**, *8*, 7115−7129.

(36) Tang, K.; Fu, L. J.; White, R. J.; Yu, L. H.; Titirici, M. M.; Antonietti, M.; Maier, J. Hollow Carbon Nanospheres with Superior Rate Capability for Sodium-Based Batteries. *Adv. Energy Mater.* **2012**, *2*, 873−877.

DOI: 10.1021/acssuschemeng.5b00403
ACS Sustainable Chem. Eng. 2015, 3, 2153−2159

(37) Xing, W.; Xue, J. S.; Dahn, J. R. Optimizing Pyrolysis of Sugar Carbons for Use as Anode Materials in Lithium-Ion Batteries. *J. Electrochem. Soc.* **1996**, *143*, 3046−3052.
(38) Zheng, T.; Xue, J. S.; Dahn, J. R. Lithium Insertion in Hydrogen-Containing Carbonaceous Materials. *Chem. Mater.* **1996**, *8*, 389−393.
(39) Alcantara, R.; Mateos, J. M. J.; Tirado, J. L. Negative Electrodes for Lithium- and Sodium-Ion Batteries Obtained by Heat-Treatment of Petroleum Cokes Below 1000 Degrees C. *J. Electrochem. Soc.* **2002**, *149*, A201−A205.
(40) Pol, V. G.; Thiyagarajan, P. Measurement of Autogenous Pressure and Dissociated Species During the Thermolysis of Mesitylene for the Synthesis of Monodispersed, Pure, Paramagnetic Carbon Particles. *Ind. Eng. Chem. Res.* **2009**, *48*, 1484−1489.
(41) Pol, V. G.; Wen, J. G.; Lau, K. C.; Callear, S.; Bowron, D. T.; Lin, C. K.; Deshmukh, S. A.; Sankaranarayanan, S.; Curtiss, L. A.; David, W. I. F.; Miller, D. J.; Thackeray, M. M. Probing the Evolution and Morphology of Hard Carbon Spheres. *Carbon* **2014**, *68*, 104−111.
(42) Ferrari, A. C.; Robertson, J. Interpretation of Raman Spectra of Disordered and Amorphous Carbon. *Phys. Rev. B: Condens. Matter Mater. Phys.* **2000**, *61*, 14095−14107.
(43) Worsley, K. A.; Ramesh, P.; Mandal, S. K.; Niyogi, S.; Itkis, M. E.; Haddon, R. C. Soluble Graphene Derived from Graphite Fluoride. *Chem. Phys. Lett.* **2007**, *445*, 51−56.
(44) Sun, Z.; Shi, X.; Wang, X.; Sun, Y. Structure and Properties of Hard Carbon Films Depending on Heat Treatment Temperatures Via Polymer Precursor. *Diamond Relat. Mater.* **1999**, *8*, 1107−1113.
(45) Huang, C. H.; Doong, R. A.; Gu, D.; Zhao, D. Y. Dual-Template Synthesis of Magnetically-Separable Hierarchically-Ordered Porous Carbons by Catalytic Graphitization. *Carbon* **2011**, *49*, 3055−3064.
(46) Gogotsi, Y. P. V. *Carbon Nanomaterials*, Second ed.; CRC Press: Boca Raton, FL, 2013.
(47) Tan, P. H.; Dimovski, S.; Gogotsi, Y. Raman Scattering of Non-Planar Graphite: Arched Edges, Polyhedral Crystals, Whiskers and Cones. *Philos. Trans. R. Soc., A* **2004**, *362*, 2289−2310.
(48) Tuinstra, F.; Koenig, J. L. Raman Spectrum of Graphite. *J. Chem. Phys.* **1970**, *53*, 1126−1130.
(49) Cancado, L. G.; Takai, K.; Enoki, T.; Endo, M.; Kim, Y. A.; Mizusaki, H.; Jorio, A.; Coelho, L. N.; Magalhaes-Paniago, R.; Pimenta, M. A. General Equation for the Determination of the Crystallite Size La of Nanographite by Raman Spectroscopy. *Appl. Phys. Lett.* **2006**, *88*, 163106.
(50) Inagaki, M.; Park, K.; Endo, M. Carbonization under Pressure. *New Carbon Materials* **2010**, *25*, 409−420.
(51) Chen, T. Q.; Pan, L. K.; Lu, T.; Fu, C. L.; Chua, D. H. C.; Sun, Z. Fast Synthesis of Carbon Microspheres Via a Microwave-Assisted Reaction for Sodium Ion Batteries. *J. Mater. Chem. A* **2014**, *2*, 1263−1267.
(52) Hong, K. L.; Qie, L.; Zeng, R.; Yi, Z. Q.; Zhang, W.; Wang, D.; Yin, W.; Wu, C.; Fan, Q. J.; Zhang, W. X.; Huang, Y. H. Biomass Derived Hard Carbon Used as a High Performance Anode Material for Sodium Ion Batteries. *J. Mater. Chem. A* **2014**, *2*, 12733−12738.
(53) Bommier, C.; Luo, W.; Gao, W. Y.; Greaney, A.; Ma, S. Q.; Ji, X. Predicting Capacity of Hard Carbon Anodes in Sodium-Ion Batteries Using Porosity Measurements. *Carbon* **2014**, *76*, 165−174.
(54) Stevens, D. A.; Dahn, J. R. The Mechanisms of Lithium and Sodium Insertion in Carbon Materials. *J. Electrochem. Soc.* **2001**, *148*, A803−A811.
(55) Stevens, D. A.; Dahn, J. R. An in Situ Small-Angle X-Ray Scattering Study of Sodium Insertion into a Nanoporous Carbon Anode Material within an Operating Electrochemical Cell. *J. Electrochem. Soc.* **2000**, *147*, 4428−4431.
(56) Stevens, D. A.; Dahn, J. R. High Capacity Anode Materials for Rechargeable Sodium-Ion Batteries. *J. Electrochem. Soc.* **2000**, *147*, 1271−1273.
(57) Komaba, S.; Murata, W.; Ishikawa, T.; Yabuuchi, N.; Ozeki, T.; Nakayama, T.; Ogata, A.; Gotoh, K.; Fujiwara, K. Electrochemical Na Insertion and Solid Electrolyte Interphase for Hard-Carbon Electrodes and Application to Na-Ion Batteries. *Adv. Funct. Mater.* **2011**, *21*, 3859−3867.
(58) Wenzel, S.; Hara, T.; Janek, J.; Adelhelm, P. Room-Temperature Sodium-Ion Batteries: Improving the Rate Capability of Carbon Anode Materials by Templating Strategies. *Energy Environ. Sci.* **2011**, *4*, 3342−3345.
(59) Alcantara, R.; Lavela, P.; Ortiz, G. F.; Tirado, J. L. Carbon Microspheres Obtained from Resorcinol-Formaldehyde as High-Capacity Electrodes for Sodium-Ion Batteries. *Electrochem. Solid-State Lett.* **2005**, *8*, A222−A225.
(60) Pol, V. G.; Pol, S. V.; Moreno, J. M. C.; Gedanken, A. High Yield One-Step Synthesis of Carbon Spheres Produced by Dissociating Individual Hydrocarbons at Their Autogenic Pressure at Low Temperatures. *Carbon* **2006**, *44*, 3285−3292.
(61) Ding, J.; Wang, H. L.; Li, Z.; Kohandehghan, A.; Cui, K.; Xu, Z. W.; Zahiri, B.; Tan, X. H.; Lotfabad, E. M.; Olsen, B. C.; Mitlin, D. Carbon Nanosheet Frameworks Derived from Peat Moss as High Performance Sodium Ion Battery Anodes. *ACS Nano* **2013**, *7*, 11004−11015.

DOI: 10.1021/acssuschemeng.5b00403
ACS Sustainable Chem. Eng. 2015, 3, 2153−2159